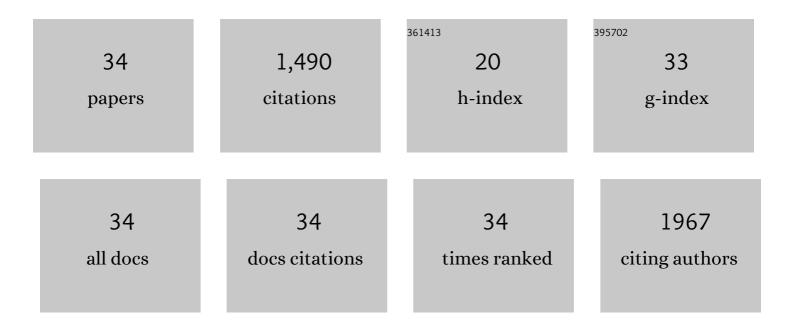
Stefan A Reinsberg

List of Publications by Year in descending order

Source: https://exaly.com/author-pdf/2862084/publications.pdf Version: 2024-02-01



#	Article	IF	CITATIONS
1	A complete distortion correction for MR images: I. Gradient warp correction. Physics in Medicine and Biology, 2005, 50, 1343-1361.	3.0	201
2	Length scale of dynamic heterogeneity in supercooled glycerol near Tg. Journal of Chemical Physics, 2001, 114, 7299-7302.	3.0	173
3	Combined Use of Diffusion-Weighted MRI and ¹ H MR Spectroscopy to Increase Accuracy in Prostate Cancer Detection. American Journal of Roentgenology, 2007, 188, 91-98.	2.2	166
4	Magnetic resonance imaging in prostate cancer: the value of apparent diffusion coefficients for identifying malignant nodules. British Journal of Radiology, 2007, 80, 90-95.	2.2	135
5	Dynamic contrast-enhanced MRI for prostate cancer localization. British Journal of Radiology, 2009, 82, 148-156.	2.2	93
6	A complete distortion correction for MR images: II. Rectification of static-field inhomogeneities by similarity-based profile mapping. Physics in Medicine and Biology, 2005, 50, 2651-2661.	3.0	86
7	Comparative study of the NMR length scale of dynamic heterogeneities of three different glass formers. Journal of Non-Crystalline Solids, 2002, 307-310, 208-214.	3.1	75
8	Metronomic gemcitabine suppresses tumour growth, improves perfusion, and reduces hypoxia in human pancreatic ductal adenocarcinoma. British Journal of Cancer, 2010, 103, 52-60.	6.4	74
9	Hyperbranched Polyglycerols as Trimodal Imaging Agents: Design, Biocompatibility, and Tumor Uptake. Bioconjugate Chemistry, 2012, 23, 372-381.	3.6	45
10	Processing of radical prostatectomy specimens for correlation of data from histopathological, molecular biological, and radiological studies: a new whole organ technique. Journal of Clinical Pathology, 2005, 58, 504-508.	2.0	41
11	The Adoption of an Open Textbook in a Large Physics Course: An Analysis of Cost, Outcomes, Use, and Perceptions. International Review of Research in Open and Distance Learning, 2017, 18, .	1.8	38
12	Heterogeneous distribution of trastuzumab in HER2-positive xenografts and metastases: role of the tumor microenvironment. Clinical and Experimental Metastasis, 2018, 35, 691-705.	3.3	38
13	Device for sectioning prostatectomy specimens to facilitate comparison between histology and in vivo MRI. Journal of Magnetic Resonance Imaging, 2010, 32, 992-996.	3.4	35
14	Analysis of Cross-Polarization Dynamics between Two Abundant Nuclei, 19F and 1H, Based on Spin Thermodynamics Theory. Journal of Magnetic Resonance, 1999, 141, 91-103.	2.1	34
15	In vivo 3T and ex vivo 7T diffusion tensor imaging of prostate cancer: Correlation with histology. Magnetic Resonance Imaging, 2015, 33, 577-583.	1.8	30
16	Solid-state1H ?19F/19F ?1H CP/MAS NMR study of poly(vinylidene fluoride). Magnetic Resonance in Chemistry, 2002, 40, 97-106.	1.9	28
17	Solid-State 19F MAS, 19F CRAMPS, and 19F → 13C CP/MAS NMR Study of an Amorphous Perfluoropolymer. Macromolecules, 2001, 34, 66-75.	4.8	26
18	Fluorine-19 NMR investigation of poly(trifluoroethylene). Polymer, 2000, 41, 3729-3736.	3.8	25

STEFAN A REINSBERG

#	Article	IF	CITATIONS
19	Solid-state 1H-static, 1H-MAS, and 1H→19F/19F→1H CP/MAS NMR study of poly(vinyl fluoride). Polymer, 2001, 42, 8137-8151.	3.8	24
20	Distortion-corrected <i>T</i> ₂ weighted MRI: a novel approach to prostate radiotherapy planning. British Journal of Radiology, 2007, 80, 926-933.	2.2	20
21	Analysis of cross-polarization dynamics between1H and19F in Viton fluoroelastomer using solid-state19F magic angle spinning and1H →19F cross-polarization magic angle spinning NMR. Magnetic Resonance in Chemistry, 1999, 37, 709-720.	1.9	19
22	Tissue Penetration and Activity of Camptothecins in Solid Tumor Xenografts. Molecular Cancer Therapeutics, 2014, 13, 2727-2737.	4.1	14
23	Dose-painted volumetric modulated arc therapy of high-grade glioma using 3,4-dihydroxy-6-[¹⁸ F]fluoro-L-phenylalanine positron emission tomography. British Journal of Radiology, 2019, 92, 20180901.	2.2	10
24	Multiâ€modal magnetic resonance imaging and histology of vascular function in xenografts using macromolecular contrast agent hyperbranched polyglycerol (HPGâ€GdF). Contrast Media and Molecular Imaging, 2016, 11, 77-88.	0.8	9
25	Fast and sensitive dynamic oxygenâ€enhanced MRI with a cycling gas challenge and independent component analysis. Magnetic Resonance in Medicine, 2019, 81, 2514-2525.	3.0	8
26	Regional radiation dose susceptibility within the parotid gland: Effects on salivary loss and recovery. Medical Physics, 2015, 42, 2064-2071.	3.0	7
27	Detecting Vascular-Targeting Effects of the Hypoxic Cytotoxin Tirapazamine in Tumor Xenografts Using Magnetic Resonance Imaging. International Journal of Radiation Oncology Biology Physics, 2009, 74, 957-965.	0.8	6
28	Rapid measurement of arterial input function in mouse tail from projection phases. Magnetic Resonance in Medicine, 2014, 71, 238-245.	3.0	6
29	Heterogeneous radiotherapy dose-outcomes response in parotid glands. Convergent Science Physical Oncology, 2018, 4, 035001.	2.6	6
30	Dynamic Contrast-Enhanced MRI. Methods in Molecular Biology, 2018, 1718, 71-87.	0.9	6
31	Dynamic contrast-enhanced MRI in mice: An investigation of model parameter uncertainties. Magnetic Resonance in Medicine, 2015, 73, 1979-1987.	3.0	5
32	Development of a method for functional aspect identification in parotid using dynamic contrast-enhanced magnetic resonance imaging and concurrent stimulation. Acta Oncológica, 2015, 54, 1686-1690.	1.8	5
33	Interhemispheric Difference Images from Postoperative Diffusion Tensor Imaging of Gliomas. Cureus, 2016, 8, e817.	0.5	2
34	Abstract 2988: Microenvironmental distribution of trastuzumab is heterogeneous and decreases sharply when administered following a single dose of bevacizumab in Her2+ve xenografts and metastases models. , 2014, , .		0